# Using Deep-Learning to Map the Solar Far-Side Magnetic Flux from Helioseismic Measurements

**S.A. Hess Webber**[1]✉, **R. Chen**[1]✉ **and J. Zhao**[1]

[1]**W. W. Hansen Experimental Physics Laboratory, Stanford University, Stanford, CA, USA;**
**Correspondence to:** ***shessweb@stanford.edu*, *rzchen@stanford.edu***

The solar far-side magnetic flux is a crucial physical quantity for space weather forecasting and solar wind modeling, but it is not currently directly observed. For about 4 years, the extreme ultraviolet (EUV) 304 Å flux of the far side was observed by STEREO/EUVI, which is used to produce proxy far-side magnetic flux maps (*talk by R. Chen, Monday*). Helioseismic far-side imaging methods are also used to produce far-side acoustic maps from near-side observations, which indirectly detect large active regions on the far side; however, these acoustic maps are not calibrated to magnetic flux. In this work, we use a deep-learning approach to produce far-side magnetic flux maps in near-real-time using near-side observations alone. Our neural network is trained on $\sim$2500 pairs (3.5 years, two pairs of maps per day) of far-side acoustic maps and magnetic flux proxy maps, and then test on the remaining half year of data. The final product can then be further calibrated to magnetic flux-transport maps for additional validation. This neural network will be applied to future far-side acoustic maps to produce near-real-time far-side magnetic flux maps, without the need for direct far-side observations.

## Background & Motivation

**Reliable, near-real-time solar far-side magnetic flux maps are important for improved modeling of the background solar wind and the solar wind structure.**

The following figure shows two synchronic maps (top) of magnetic field, one from data assimilation using only a flux transport model (FTM) [6] and the other after manually incorporating a large AR on the modeled data at the location of new emergence. The synchronic maps are used to calculate maps of Squashing factor Q (Q-maps; middle) [7] at a distance of 2.5 $R_{sun}$, employing a potential field source surface (PFSS) model [*e.g.* 1; 3; 5]. Q-maps effectively show magnetic topology. Lanes between opposite-sign (blue and red) regions in the maps represent current sheets (helmet streamers). Those between same-sign (same color) regions represent coronal hole boundaries (pseudo-streamers). The new active region (AR) changes the coronal structure significantly: altering the shapes of the existing pseudo-streamers (B and C), and generating a new pseudo-streamer (D). The "existing" and new pseudo-streamer are compared side-by-side with SOHO/LASCO C2 observations (bottom).

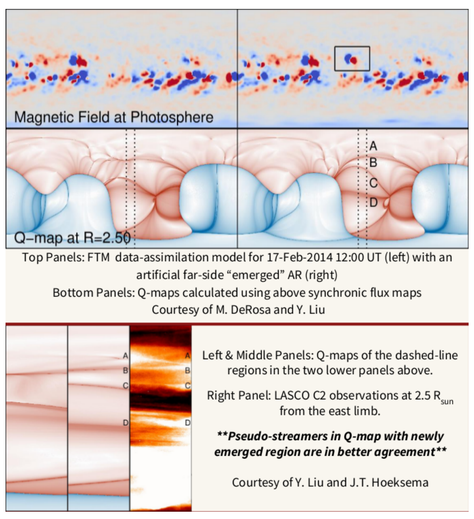


**Flux transport models.** FTMs effectively progress observed near-side magnetic flux around to the solar far side. They provide reasonable approximations of the synchronic, full-sun signed flux based on assimilated magnetic data. Unfortunately, **FTMs are incapable of incorporating either the growth of existing ARs or the emergence of new magnetic flux.**

**Far-side observations.**
There is a quantitative relationship between 304 Å EUV emission and magnetic flux [8]. The STEREO/SECCHI EUVI instruments provide several years of far-side 304 Å observations (see example **below, bottom**). However, the STEREO spacecraft have already orbited back around to a separation angle $<90°$ with Earth. Furthermore, communications with STEREO B were permanently lost in Oct 2014, just before it passed behind the Sun. No current or planned missions have orbital positions conducive to consistent observations of the solar far side, either for magnetic fields or EUV proxies. **There is no guarantee of future observations.**

**STEREO A & B spacecraft as of 2019-Sep-12 21:00 UT**

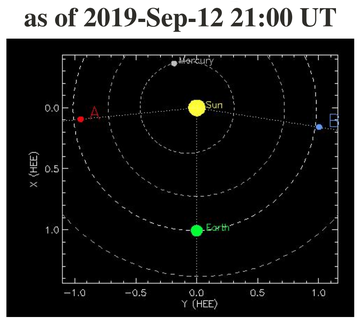


Credit: STEREO Science Center

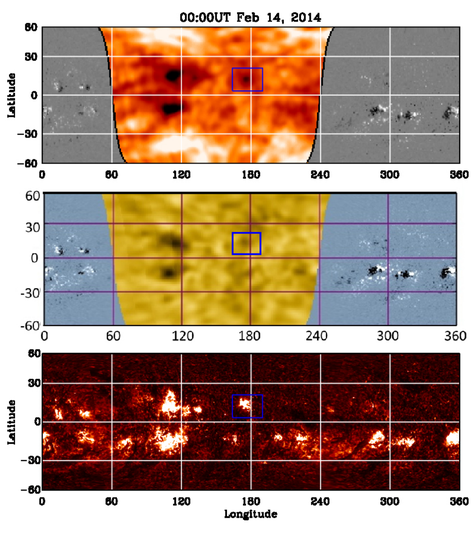


**Helioseismic imaging.** Helioseismic techniques are also used to image the far side. These techniques include acoustic holography (middle) [2; 4] and time-distance methods [9]. These maps show the location and size of far-side ARs, but both methods often give spurious signals. We recently developed a new time-distance technique that increases the acoustic resolution of the far side maps (top) [10]. However, all acoustic maps are measures of wave travel-time perturbations. **None of these data are calibrated into magnetic flux.**

## Data & Preparation

There are several overarching steps necessary to calibrate acoustic maps to far-side magnetic flux maps: (**bold teal** indicates focus of poster)

1. Generate far-side acoustic travel-time maps ✓✓
2. Use deep neural net to learn relationship between EUV and magnetic flux – using near-side images ✓✓
3. **Apply learned EUV⇔magnetic-flux relationship to far-side EUV images to get far-side magnetic flux proxy images** ✓
4. **Use deep neural net to learn relationship between far-side magnetic-flux proxy and far-side acoustic maps (current)**
5. Apply learned far-side acoustic⇔magnetic-flux-proxy relationship to near-real-time acoustic maps

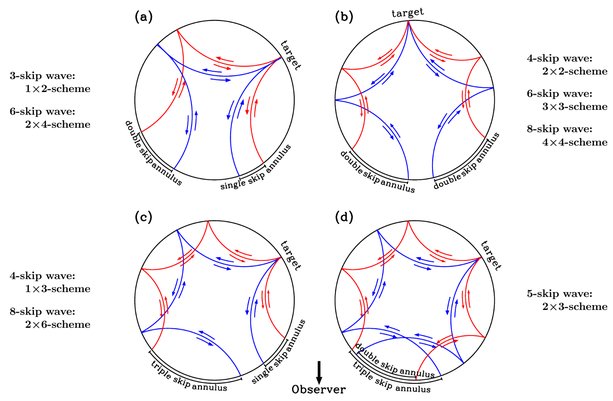


**Producing far-side acoustic maps.** Waves that get reflected within a far-side AR experience a reduction in their total travel times, which can be measured using near-side waves to show the location, size, and perhaps magnetic-field strength of the far-side AR. Our new far-side time-distance technique takes advantage of helioseismic geometry for different "skip" waves (number of surface reflections; *e.g.*, some 6- and 8-skip waves have the same far-side sensitivity geometry as 4-skip 2x2-scheme waves). We ultimately use 14 total sets of individual wave measurements to build up maps of acoustic wave travel-times across the far-side of the solar disk. The higher acoustic resolution requires less time-averaging for reliable signal-to-noise.

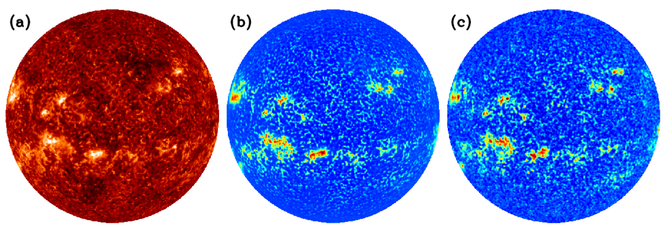


**Machine learning between SDO/AIA and SDO/HMI.** In order to convert *far-side* EUV 304 Å images to magnetic flux proxy data, we first train on corresponding *near-side* EUV 304 Å and magnetic flux images. We use a Unet deep learning architecture, trained on 4 image pairs of EUV and magnetic flux per day using 8 years of data from 2010-May 1 to 2018-Apr-30, a total of $\sim$11,000 examples. Data are split into a training set, devel. set (4%), and test set (4%). 15 days are blocked before and after each devel./test set, to prevent the same ARs from appearing in both the training set, and development and test sets. **The trained deep neural network reproduces the magnetic flux in great detail from the EUV 304 Å flux, with a correlation of about 0.9.** The above example shows (a) an AIA 304 Å image (input), (b) the learned magnetic-flux proxy image (output), and (c) the actual HMI magnetic flux image (target).

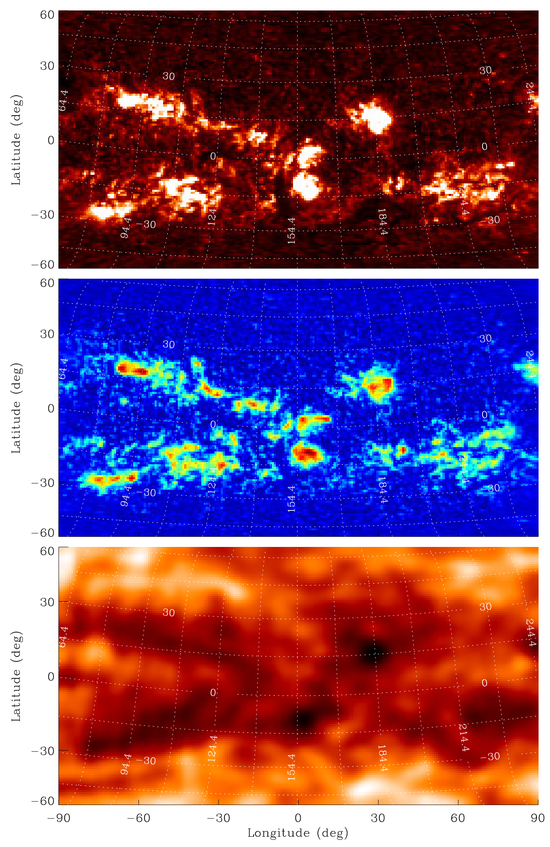


**Prepped far-side data.** Our far-side data sets are STEREO A & B EUVI 304 Å images (top), **derived STEREO A & B magnetic-flux proxy images (middle), and far-side acoustic images (bottom)**; this example is from 2014-May-13 00:00 UT. Both time-series range from 2010-May-13 00:00 UT–2014-Aug-18 12:00 UT (limited by availability of STEREO data). We include 2 observations per day (midnight & noon; UTC). After "bad" data are removed from the training set (partial images, flare occurrences, *etc.*), we ultimately train on a total of $\sim$2500 pairs of images. Our maps have dimensions of 255×121 (limited by the spatial resolution of acoustic maps). All images are in the form of far-side Carrington maps, using Carrington longitude (central meridian fixed at 0°; between $\pm$90°) and sin(latitude) between $\pm$60°. STEREO EUVI images have been: 1) calibrated through the SSW IDL routine *SECCHI_prep.pro* (with optional rotation and smask corrections), 2) scaled to AIA 304 Å flux (including AIA sensitivity degradation), 3) merged (A & B) to create one far-side Carrington map per time step, 4) transformed into magnetic-flux proxy images using machine-learned algorithm, and 5) pixel-scaled to match acoustic data parameters (*e.g.,* pixel size).

## Machine Learning Framework

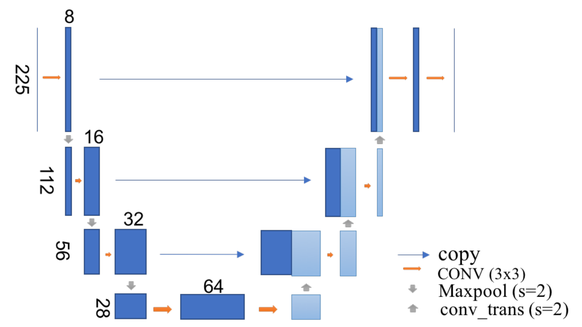


**Unet deep neural network architecture.** For the far-side data, we use a Unet neural network model similar to that used for the near-side EUV⇔magnetic-flux training algorithm. **Unet combines local and global spatial information effectively.** Because of the relatively small training set and the lower dimensionality of the images, we use fewer convolutional layers in this framework than were used for the near-side architecture. A rectified linear unit (ReLU) non-linear mapping is applied after each 3×3 convolution, followed by a 2×2 maxpool downsampling. Through each downsampling step, feature channels are doubled. After the lowest convolutional layer, 2×2 convolutional upsampling is applied. Between each upsampling step, we concatenate the upsampled and downsampled channels of that convolutional layer, and perform a 3×3 convolution followed by a ReLU. Through each upsampling step, feature channels are halved. The final output map has the same dimensions as the original input map.

## Initial Results

**Note, these results are *very* preliminary! We have not yet compared between the output predictions and target images, or tweek our initial Unet framework to improve performance. However, the results are promising!**

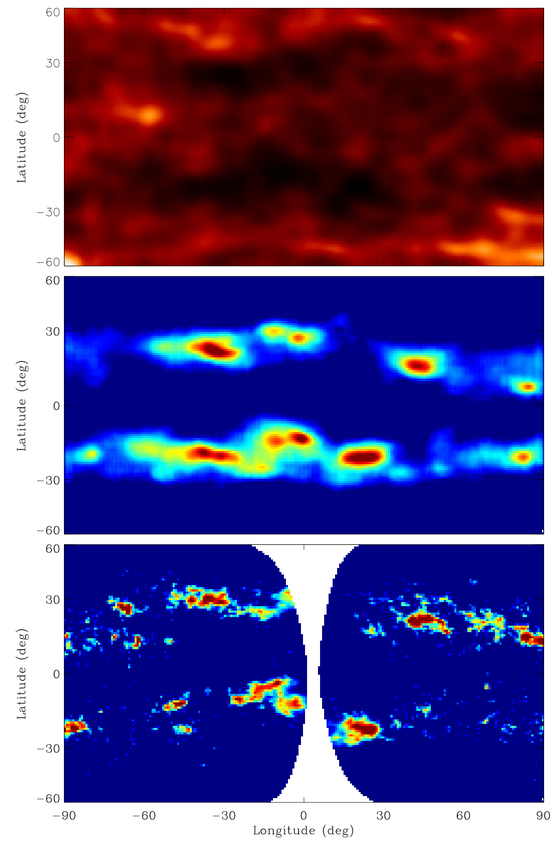


**ML input, output, and target.** The results shown here are from the first training attempt between our input and target data sets, using the ML framework above. These maps correspond to the solar far-side on 2011-Sep-24 12:00 UT. The output magnetic-flux map predicted by our trained algorithm (middle) has the same spatial resolution as the input acoustic map (top). **The general shapes, sizes, and locations of the predicted ARs, as well as the field strength of the larger ARs, correspond reasonably well with the target magnetic-flux proxy map** (bottom). The gap in the center of the target map is due to the separation angle between STEREO A & B at the time. This region of missing observations has been masked out of the loss function using an appropriate weighting scheme.

## Next Steps

- Determine statistics for initial training iteration
- Tweek initial Unet framework to improve performance
- Finalize far-side data preparation
- Apply learned far-side acoustic⇔magnetic-flux-proxy relationship to all acoustic maps (May 2010–present, continued into future).
- Develop associated uncertainty maps

## References

[1] M. D. Altschuler and G. Newkirk. Magnetic Fields and the Structure of the Solar Corona. I: Methods of Calculating Coronal Fields. *Solar Phys.*, 9(1):131, 1969.

[2] D. C. Braun and C. Lindsey. Seismic Imaging of the Far Hemisphere of the Sun. *Astrophys. J. Lett.*, 560:L189, 2001.

[3] J. T. Hoeksema, J. M. Wilcox, and P. H. Scherrer. Structure of the heliospheric curent sheet in the early portion of sunspot cycle 21. *J. Geophys. Res.*, 87(A12):10331, 1982.

[4] C. Lindsey and D. C. Braun. Seismic images of the far side of the sun. *Science*, 287(5459):1799, 2000.

[5] K. H. Schatten, J. M. Wilcox, and N. F. Ness. A model of interplanetary and coronal magnetic fields. *Solar Phys.*, 6(3):442, 1969.

[6] C. J. Schrijver and M. L. DeRosa. Photospheric and heliospheric magnetic fields. *Solar Phys.*, 212 (1):165, 2003.

[7] V. S. Titov. Generalized Squashing Factors for Covariant Description of Magnetic Connectivity in the Solar Corona. *Astrophys. J.*, 660(1):863, 2007.

[8] I. Ugarte-Urra, L. Upton, H. P. Warren, and D. H. Hathaway. Magnetic Flux Transport and the Long-Term Evolution of Solar Active Regions. *Astrophys. J.*, 815(2):90, 2015.

[9] J. Zhao. Time-Distance Imaging of Solar Far-Side Active Regions. *Astrophys. J. Lett.*, 664(2): L139, 2007.

[10] J. Zhao, D. Hing, R. Chen, and S. A. Hess Webber. Imaging the Sun's Far-Side Active Regions Using Multiple Measurement Schemes of Multi-Skip Acoustic Waves. *In Prep.*, 2019.